1 **Employing the synergistic effect between aquaporin nanostructures and graphene oxide for**

2 **enhanced separation performance of thin-film nanocomposite forward osmosis membranes**

3

4 Nawshad Akther[a], Victoria Sanahuja-Embuena[b,c], Radosław Górecki[b,c], Sherub Phuntsho[a], Claus

5 Helix-Nielsen[b] and Ho Kyong Shon[a]*

6

7 [a] School of Civil and Environmental Engineering, University of Technology Sydney (UTS), NSW

8 2007, Australia

9 [b] Department of Environmental Engineering, Technical University of Denmark, Bygningstorvet

10 115, 2800 Kongens Lyngby, Denmark

11 [c] Aquaporin A/S, Nymøllevej 78, 2800 Kongens Lyngby, Denmark

12

13 * Corresponding author: Prof. Hokyong Shon Email: hokyong.shon-1@uts.edu.au; Tel.: +61 2

14 9514 2629; Fax: +61 2 9514 2633.

15

16 **Keywords:** Membrane; thin-film nanocomposite (TFN); graphene oxide (GO); aquaporin,

17 forward osmosis (FO)

18   **Abstract**

19   In this study, novel thin-film nanocomposite (TFN) membranes were developed by incorporating

20   graphene oxide (GO) and Aquaporin Z (AqpZ) reconstituting nanostructure (AQN) into the

21   polyamide (PA) active layer to improve the forward osmosis (FO) performances of the PA TFN

22   membranes. First, the AQN loading in the PA layer was optimized, followed by the GO addition

23   in PA layer at various loadings until the optimal FO process performance was attained.

24   Experimental results showed that GO flakes increased membrane water flux but decreased

25   selectivity by creating non-selective voids in PA layer. Whereas, AQN increased membrane

26   selectivity by healing the non-selective PA defects created by the GO flakes. The synergistic effect

27   of GO-AQN improved the water flux without deteriorating the selectivity of the membrane. The

28   TFN membrane with 0.2 wt% AQN and 0.005 wt% GO loading (TFN50) showed almost 3 folds

29   increase in water flux (24.1 $L.m^{-2}.h^{-1}$) in comparison to the TFC membrane (8.2 $L.m^{-2}.h^{-1}$), while

30   retaining the membrane selectivity (0.37 $g.L^{-1}$). Interestingly, the TFN50 membrane demonstrated

31   a 27% lower specific reverse salt flux (*SRSF*) and a marginal increase in water flux than the TFN

32   membrane embedded with 0.005 wt% GO and no AQN (TFNGO50). The overall experimental

33   results confirmed that the addition of AQN into GO-based PA TFN membranes could improve the

34   membrane selectivity by reducing the non-selective PA defects created by GO flakes. The results

35   of this study could provide strategies to further enhance the selectivity of GO-based TFN

36   membranes by preventing the formation of defective PA layer.

37

1 Introduction

Over the recent years, membrane separation operations have been recognized as a potential alternative to traditional processes owing to the possible benefits of their excellent separation efficiencies, and lower operating and capital costs [1-4]. Since membrane processes that are osmotically-driven like forward osmosis (FO) possess higher water recovery and lower fouling tendency as opposed to pressure-driven membrane processes like reverse osmosis (RO), they have been intensely investigated for wastewater treatment [5], brine dilution [6], food processing [7] and resource recovery [8]. The main driving force in FO processes is the osmotic pressure difference existing between the feed solution (FS) and the more concentrated draw solution (DS), which allows water to flow across the semi-permeable membrane [3, 9]. Consequently, FO processes have been found to consume lower energy than RO when employed in applications requiring DS regeneration.

FO processes mainly rely on polyamide (PA) thin-film composite (TFC) membranes, which are prepared from the interfacial polymerization (IP) reaction between trimesoyl chloride (TMC) and m-phenylenediamine (MPD), due to their superior permeability-selectivity performance, and broader pH tolerance range than that of the cellulose-based membranes [10, 11]. The porous substrate of the TFC membrane provides mechanical support to the dense and ultrathin PA selective layer, which influences the separation performance of the membrane. Although PA TFC membranes are currently recognized as the state-of-the-art membranes for use in wastewater treatment, desalination and other separation applications, they exhibit low water flux, and a trade-off between water permeability and solute selectivity, which significantly inhibits the process separation efficiency [12]. In addition, the inherently hydrophobic and rough surface of the PA layer

3

61 promotes membrane fouling, which could impede their application for high-fouling wastewater

62 treatment [13]. The declined membrane performance could reduce membrane life and increase the

63 overall operating costs [14, 15]. Hence, the development of highly efficient PA TFC FO

64 membranes is required to enhance the membrane performance and reduce the foulant deposition

65 on the membrane surface.

66   To overcome the issues mentioned above, thin-film nanocomposite (TFN)

67 membranes, which involves the addition of nanomaterials into the PA selective layer, have

68 been extensively explored for enhancing the membrane separation efficiency [11, 12, 16].

69 Since first reported by Hoek's group in 2017 [17], various nanomaterials like zeolites [18],

70 carbon nanotubes [19], graphene oxide (GO) [20, 21], graphene quantum dots [22, 23],

71 silica [4, 24], covalent/metal-organic frameworks [25, 26] and titanium oxide [27] have

72 been heavily studied for altering the membrane characteristics and performance depending

73 on the physical and chemical properties of the embedded nanomaterial. For instance, porous

74 nanomaterial like zeolites act as molecular sieves for size-selective separation of molecules

75 and are suitable for pervaporation and gas separation [28]; whereas, two-dimensional GO

76 flakes have been widely used to improve the membrane hydrophilicity, antifouling and

77 antimicrobial properties for desalination and wastewater treatment [29-31].

78   Nonetheless, TFN membranes often exhibit lower solute rejection compared to the

79 TFC membranes due to the formation of non-selective interfacial voids between the

80 nanoparticles and PA matrix. The defective non-uniform PA layer in TFN membranes form due

81 to several reasons, such as the incompatibility of the nanofillers with the PA matrix, severe

82 aggregation of nanofillers within the PA, and nanofillers impeding the reaction between monomers

83 during the IP process [12, 20]. Therefore, it is imperative to select nanomaterials that are

84   compatible with the PA and to design TFN membranes to improve the membrane water

85   permeability without significantly deteriorating the selectivity.

86   It has been recently observed in one of our studies that GO flakes created non-selective

87   patches when incorporated into the PA layer of the membrane [20], which reduced the membrane

88   selectivity. To tackle this issue, this study considered the use of nanostructures incorporating

89   aquaporin proteins, specifically Aquaporin Z (AqpZ). AqpZ is a transmembrane protein in charge

90   of selective transport of water through the cell membrane of Escherichia coli (E. coli). It is formed

91   by a bundle of six α helices, which leave a narrow opening inside, allowing only water molecules

92   to pass through [32-34]. Thus, AqpZ were extensively studied to be used in membrane technology

93   for developing advanced biomimetic membranes that could be more selective than conventional

94   TFC membranes [35-37]. Since AqpZ can degrade or denature, they require a membrane cell

95   structure or similar to function properly when embedded into the polymer membranes.

96   Stabilization of these proteins is mostly done by incorporating them into the bilayer membranes

97   of vesicular nanostructures, such as liposomes made of phospholipids or polymersomes made of

98   amphiphilic block copolymers [38-40]. There is a preference of using polymer-based

99   nanostructures for stabilization of AqpZ as they are better suited in terms of stability for membrane

100   manufacturing processes and industrial applications [41, 42]. To further improve the incorporation

101   of these nanostructures into the membrane, amino terminated chains could be introduced as they

102   can covalently bond the nanostructures within the PA layer [43, 44]. Therefore, in this study, we

103   used AqpZ incorporated in Pluronic® based nanostructures of poly(ethylene glycol)-block-

104   poly(propylene glycol)-block(polyethylene glycol) (PEG-PPG-PEG) blend with poly(ether

105   monoamine) (PMA). The PMA could facilitate the addition of nanostructures into the PA layer

106   during the IP reaction, and AqpZ proteins will assist in maintaining the selectivity that may be lost

107   from the incorporation of GO flakes.

108   To the best of our knowledge, this is the first study to present the synergistic use of AqpZ

109   reconstituting nanostructure (AQN) with GO for the preparation of PA TFN membranes.

110   Additionally, it is the first to describe the "healing" effect of AQN towards the non-selective

111   defects created by GO flakes in the PA layer. We believe that the article will open the doors

112   towards further research of the synergistic use of different nanostructures for the preparation of

113   novel membrane materials.

114   **2   Experimental**

115   **2.1   Chemicals**

116   Commercial GO-water dispersion (particle size <10 μm, 4 mg.mL^{-1}) was supplied by

117   Graphenea; and the GO properties and characteristics can be found on the supplier's website.

118   Membrane substrates were prepared from polysulfone pellets (PSf, P-3500 Udel$^{®}$, Solvay) using

119   1-methyl-2 pyrrolidone (NMP, ≥ 99.5%, Merck) as the polymer solvent. Trimesoyl chloride (TMC,

120   98%) and m-phenylenediamine flakes (MPD, 99%) were provided by Sigma-Aldrich. N-hexane

121   (98.5%, Merck) was used as an organic solvent for TMC. Sodium chloride (NaCl, > 99.7%, Chem

122   Supply) was utilized as a draw solute. Deionized (DI) water (Milli-Q®, Merck) with a resistivity

123   of ~18 MΩ.cm^{-1} was used to prepare DS and FS. Polymer-based nanostructure solution

124   incorporated with AqpZ was developed by and obtained from Aquaporin A/S (Denmark). The

125   development and characteristics of the nanostructure solution can be found in the corresponding

126   patent and our previous work [35, 45].

2.2 Membrane preparation

The porous flat sheet substrates were prepared from 12 wt% PSf dope solution using the phase inversion technique as described in our previous work [20]. More details are given in Section S1 of the Supplementary Information (SI). IP was then conducted on the prepared PSf substrates to produce TFC membranes. First, the substrate was treated with 2 wt% MPD aqueous amine solution for 2.5 min and the excess amine solution was removed using a nitrogen knife. The amine-saturated substrate was then exposed to 0.1 wt% TMC organic solution for 1 min to initiate the IP reaction. More information is provided in the SI. The AQN and GO incorporated TFN membranes were produced using the same procedure as that of TFC membrane, except for the addition of AQNs and GO flakes in the MPD aqueous solution at the desired loadings. The GO flakes were first added to the amine solution and placed in a bath sonicator for 30 min to achieve uniform dispersion. AQNs were then added to the well-dispersed GO-containing amine solution and mixed for 1 h using a shaker, which was brought in contact with the PSf substrate. The subsequent amine-impregnated PSf substrate was reacted with TMC organic solution to produce the TFN membrane. **Table 1** presents the AQN and GO loadings in MPD amine aqueous solution of the various membranes prepared in this study.

144 **Table 1** AQN and GO compositions of the pristine TFC and modified TFN membranes.

Membranes	Concentration in aqueous amine solution	
	AQN (g.L^{-1})	GO (mg.L^{-1})
TFC	0	0
TFN0	2	0
TFN25	2	25
TFN50	2	50
TFN75	2	75
TFNGO25	0	25
TFNGO50	0	50
TFNGO75	0	75

145

2.3   Membrane characterization

147   Membrane surface morphology was studied using a scanning electron microscope (SEM,

148 Zeiss Supra 55VP) and atomic force microscopy (AFM, Park XE7, Park Systems). Dry samples

149 of the membranes were sputter-coated with an 8 nm thick Pd/Au layer before SEM investigation

150 and examined at 5 or 10 kV. AFM scanning was repeated at least three times for each sample under

151 tapping mode with a scan area of 5 µm × 5 µm and the average surface roughness measurements

152 were reported. The surface chemistry of the TFC and TFN membranes were examined using

153 Fourier transform infrared spectroscopy (FTIR, Shimadzu MIRacle 10). An optical tensiometer

154 (Attension Theta Lite 100, Biolin Scientific) was used to verify the membrane surface

155 hydrophilicity by randomly measuring at least seven water contact angles on the surface of each

156 membrane sample and the average value was reported. The charge on the membrane surface was

157 determined over a pH range of 3 to 10 by measuring the zeta potential using an electrokinetic

158 analyzer (SurPASS^{TM} 3, Anton Paar). The gap height of the membrane sample holder was adjusted

8

159   to approximately 100 µm, and 1 mM KCl solution was used as the electrolyte. The electrolyte pH

160   was varied using 0.05 M NaOH and HCl. The membrane surface zeta-potential was verified from

161   the acquired streaming potential.

162   **2.4   Membrane performance evaluation**

163   As previously described in our work [25], a lab-scale FO setup was utilized to ascertain the

164   membrane performance. During the FO tests, both the DS and FS were co-currently circulated

165   across the membrane at a flow rate of 0.5 L.min^{-1} (12.6 cm.s^{-1}), unless stated otherwise, and their

166   temperature was maintained at 22 °C using a temperature controller. The membranes were placed

167   in AL-FS (active layer facing FS) orientation while using DI water and 0.5 M NaCl as FS and DS,

168   respectively. The water flux (J_w, L.m^{-2}.h^{-1}) and reverse solute flux (J_s, g.m^{-2}.h^{-1}) through the

169   membrane was determined from Eqs. (S1) and (S2), respectively. The water and reverse solute

170   flux values were employed to evaluate the specific reverse solute flux ($SRSF$, g.L^{-1}) across the

171   membrane to indicate the membrane selectivity (Eq. S3). Section S2 of the SI presents the

172   equations that are employed to calculate the membrane performance parameters.

173   The non-linear regression model developed for FO membranes [16] was used to establish

174   the pure water permeability coefficients (A, L.m^{-2}.h^{-1}.bar^{-1}), solute permeability coefficients (B,

175   L.m^{-2}.h^{-1}) and intrinsic selectivities (B/A, bar^{-1}) of the membranes.

176   **3   Results and discussion**

177   **3.1   Membrane characterization**

178   In this study, AQNs and GO flakes were embedded in the PA layer to improve the separation

179   performance of the PA TFN FO membranes. The FTIR spectra shown in **Fig. 1** were used to assess

9

180   the surface chemistry of the prepared membranes. The spectra show distinctive fingerprints of the

181   TFC and TFN membranes arising from their PA selective layers and PSf substrates [46]. The

182   typical peaks showing the functional groups of the PSf substrate occur at 1294 cm^{-1} (asymmetric

183   O=S=O bond stretching vibration), 1151 cm^{-1} (symmetric O=S=O bond stretching vibration),

184   1504 cm^{-1} (aromatic in-plane ring stretching vibration), 1246 cm^{-1} (asymmetric C–O–C stretching

185   vibration) and 1385 cm^{-1} (symmetric C–H deformation) [31, 46]. The distinctive peaks denoting

186   the functional groups of PA appear at 1657 cm^{-1} (C=O stretching, C–N stretching, and C–C–N

187   deformation vibration in the secondary amide group of amide I band), 1608 cm^{-1} (C=C ring

188   stretching or N–H deformation vibration in aromatic amide), and 1541 cm^{-1} (C–N stretching and

189   N–H in-plane bending vibration in the –CO–NH– group of the amide II band) [46, 47]. The TFN50

190   membrane showed the most intense peaks at 2848 cm^{-1} (symmetric C–H stretch), and 2918 cm^{-1}

191   (asymmetric C–H stretch) due to the presence of GO flakes in the PA layer [20, 48]. The broad

192   absorption band from 3150 to 3750 cm^{-1} arises from the overlapping peaks attributed to the PA

193   structure's carboxyl group and N–H stretching, and GO flakes' hydroxyl group stretching. As a

194   result, the TFN50 demonstrated the most substantial peak at 3310 cm^{-1} owing to the existence of

195   ample O–H groups from the GO flakes. Other groups related to the AQNs like C–H and N–H are

196   found within the same range as that of the PSf and PA. The high intensity of these peaks masks

197   those of the AQNs as they are present in low concentration; thus, making FTIR only a supporting

198   analysis for identifying AQN incorporation. Even though some traces can be found indicating the

199   presence of the AQNs, other analysis like membrane performance is more precise in displaying

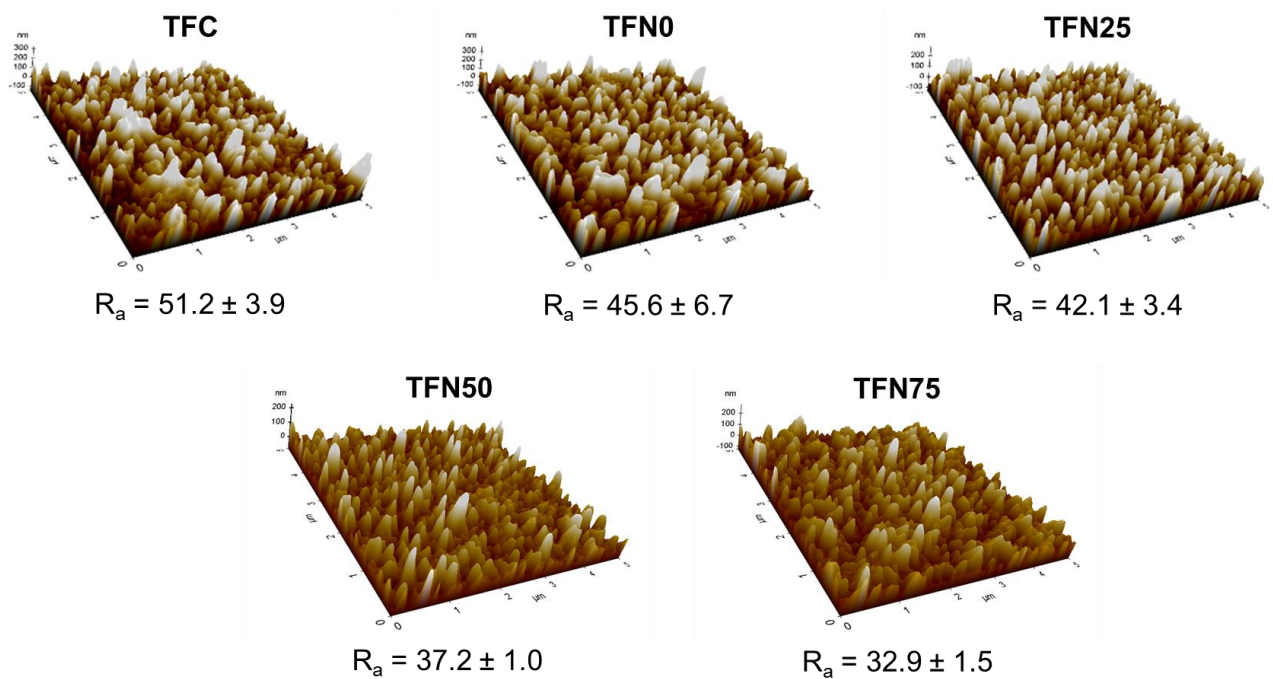200   the effect and incorporation of the AQNs.

201
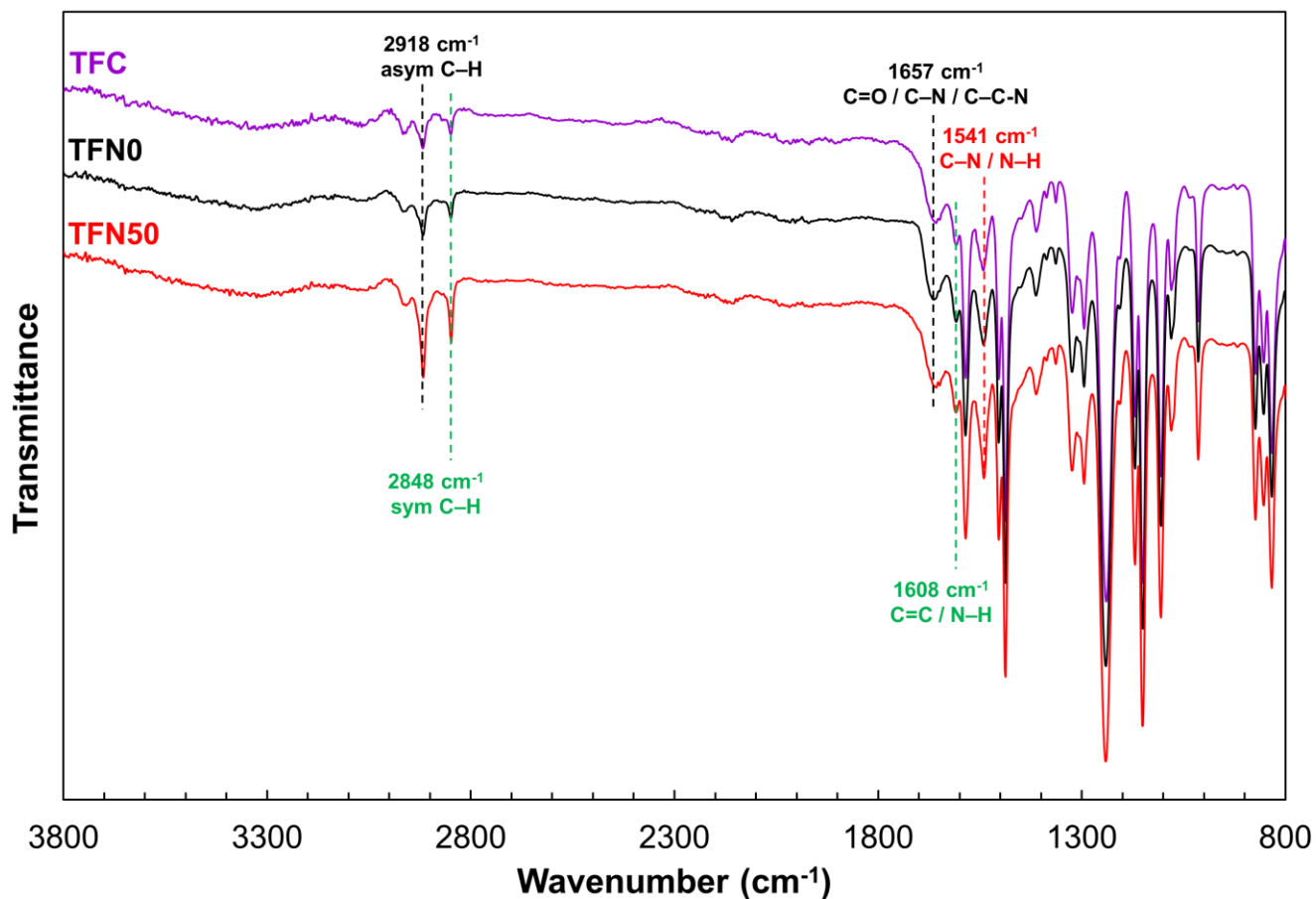
Fig. 1: FTIR spectra of the pristine TFC and modified TFN membranes.

The surface roughness of the TFC and TFN membranes was examined using the AFM topography. **Fig. 2** presents the AFM images of the fabricated TFC and TFN membranes, along with the mean membrane roughness (R_a). The root mean square (R_q) and maximum (R_{max}) membrane surface roughness values are presented in Table S1 of the SI. The TFC membrane exhibited the roughest PA surface with a R_a value of 51.2 nm. The R_a value reduced to 45.6 nm for TFN0 membranes due to incorporation of AQNs. Addition of GO significantly decreased the membrane surface roughness due to GO restricting the PA growths during the IP reaction. The membrane surface smoothness increased with an increase in GO flake loading due to more

11

213   effective retardation of MPD diffusion into the TMC/n-hexane organic phase. As a result, the

214   TFN75 membrane revealed the smoothest surface ($R_a = 32.9$ nm) as the GO sheets at a loading of

215   75 mg.L^{-1} slowed down the IP reaction most effectively; thus, forming smaller PA protrusions.

216

TFC	TFN0	TFN25
$R_a = 51.2 \pm 3.9$	$R_a = 45.6 \pm 6.7$	$R_a = 42.1 \pm 3.4$

| TFN50	TFN75
$R_a = 37.2 \pm 1.0$	$R_a = 32.9 \pm 1.5$

217

218

219   **Fig. 2**: AFM images representing the PA surface roughness of the prepared TFC and TFN
220   membranes. Error bars represent one standard error obtained from roughness measurements of at
221   least three membrane samples for each condition.

222

223   The PA surface and the membrane cross-section morphologies were examined using SEM

224   as shown in **Fig. 3**. All the membranes demonstrate the characteristic ridge-and-valley structures

225   of the PA layer. Both the TFC and TFN0 membranes display a consistent distribution of the PA

226   ridge-and-valley structures. Nonetheless, the PA structure of the pristine membrane shows

227   compact globule-like formations; whereas, that of TFN0 is sparse with leaf-like formations. The

228 AQNs compete with MPD as they can covalently bond with TMC via the amine groups of PMA

229 chains during the IP reaction. We speculate that since less MPD is able to react with TMC,

230 incorporation of AQNs into the PA layer should reduce the PA cross-linking density and form

231 sparser leaf-like structures compared to the TFC membrane. Additionally, AQNs consisting of

232 PEG-PPG-PEG may affect the diffusion of MPD to the organic phase, which further alters the

233 morphology of the PA layer.

234

235
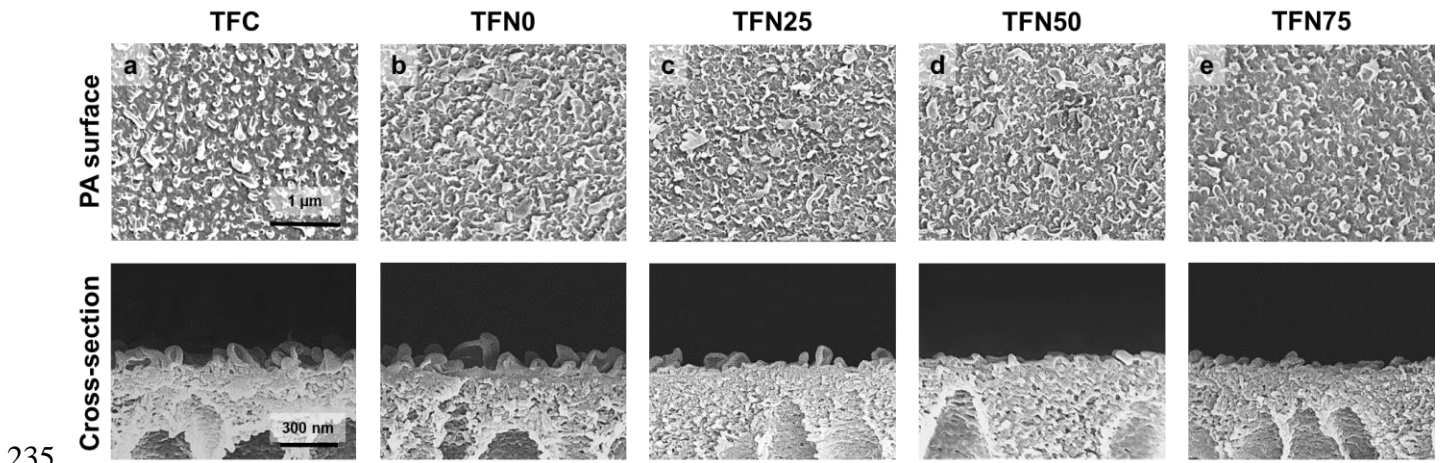
236 **Fig. 3**: SEM images demonstrating both the surface morphology of the PA layer (top) and cross-
237 section of the prepared membranes (bottom): (a) pristine TFC, (b) TFN0, (c) TFN25, (d) TFN50
238 and (e) TFN75.
239

240   Interestingly, the incorporation of GO flakes into the PA layer considerably transformed the

241 membrane morphology by forming much smaller ridges and smoother PA layer than those of the

242 pristine TFC and TFN0 membranes as evident from their AFM and SEM surface morphology

243 images (**Fig. 2** and **Fig. 3**). As discussed in our previous study, GO-incorporated TFN membranes

244 exhibited smoother PA surfaces compared to the TFC membranes because GO flakes prevented

245 MPD from quickly diffusing into the TMC organic phase during the IP process [20]. As a result,

246 the IP reaction is delayed due to the effect of steric hindrance resulting from the GO flakes. GO

247 can further reduce the reaction rate between MPD and TMC by preferentially reacting with the

248 oxygen functional groups of both the monomers.

249 It can be observed from the cross-sectional SEM images that the height of the PA layer

250 decreased on addition of AQNs and GO flakes (**Fig. 3**). The PA layer height here does not indicate

251 the PA skin thickness but the average PA layer height from the top of the substrate to the PA ridge.

252 The average PA layer height obtained from the SEM images is presented in **Fig. 4**. Both AQNs

253 and GO flakes decreases the average PA layer height by intruding the development of PA ridge-

254 and-valley formations during the IP reaction through steric hindrance and by reacting with the acyl

255 chloride groups of TMC [49]. Consequently, the overall thickness of the PA layer diminishes with

256 increasing GO flake loading.

257
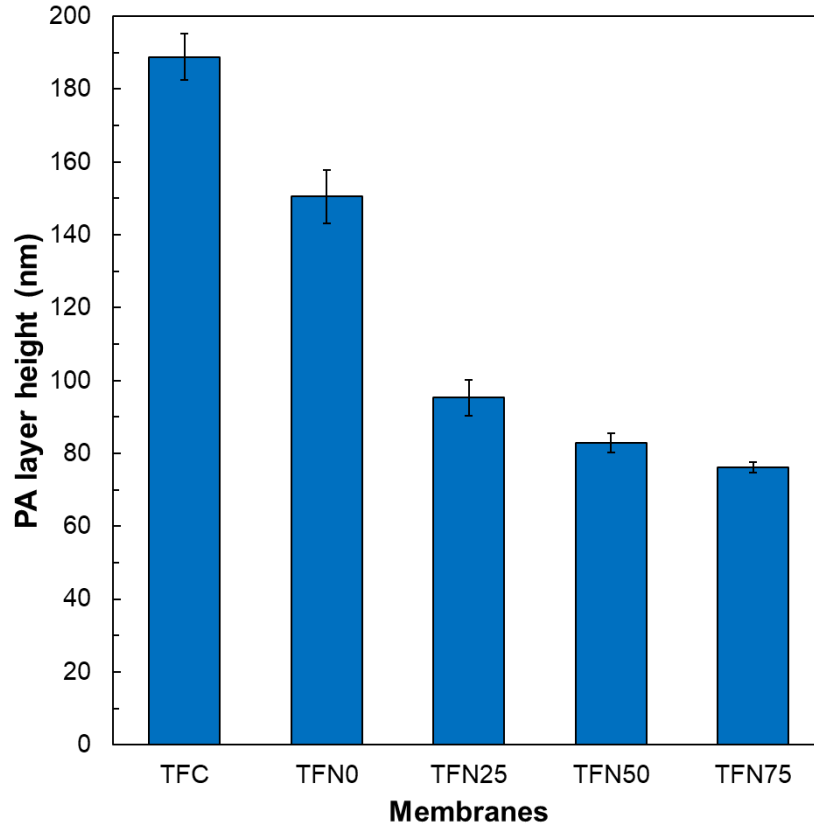
Fig. 4: PA layer height of the prepared pristine TFC and modified TFN membranes. Error bars represent one standard error obtained from at least three measurements for each membrane sample.

The membrane surface hydrophilicity was established from water contact angles measured at the air-water interface on the PA layer surface. As displayed in **Fig. 5**a, the mean water contact angles on the TFN0 surface was higher than that of the TFC membrane, suggesting that AQNs decrease the membrane surface wettability. AQNs used in this study contain the amino terminated PMA to allow covalent bonding within the PA layer. PMA is hydrophobic and its incorporation explains the increase in the contact angles measurements for TFN0. Additionally, AQNs have a hydrophobic part for the AQNs to stabilize in the membrane bilayer of the vesicle or nanostructures. The hydrophobic PMA chains may be exposed within the PA if the AQN is damaged during IP

15

271 reaction, which can increase the hydrophobicity of the TFN0 membrane regardless of AQNs

272 increasing the membrane permeability. In contrast, the water contact angles on the TFN membrane

273 surfaces substantially decreased from 85.4° for the AQN-embedded TFN0 membrane to 71.3°,

274 63.2°, and 55.9° for the AQN-GO-embedded TFN25, TFN50 and TFN75 membranes, respectively,

275 which confirms the improvement in membrane hydrophilicity after GO addition in the PA layer.

276 The enhanced wettability of the GO-embedded TFN membranes could be attributed to the

277 hydrophilic oxygen-containing functional groups of GO. Membrane surface hydrophilicity is

278 considered to be an essential membrane property in assessing the membrane performance as it can

279 influence both the water permeability and fouling behaviour of the membranes [50].

280   The surface charges of the TFC and TFN membranes were ascertained over a pH range of 3

281 to 10 by evaluating their surface zeta potentials. As can be seen from **Fig. 5**b, all membrane

282 surfaces were negatively-charged at pH greater than 5 because of the deprotonation of the PA

283 layer's carboxyl and amino functional groups [51]. The membrane surfaces become positively-

284 charged at a lower pH due to the protonation of the end amino groups in the PA. The negative

285 surface charge of TFN membranes augmented at a higher GO concentration owing to the oxygen-

286 containing groups of GO that heighten the negative charges by deprotonating in alkaline conditions.

287 **Fig. 5**b shows the isoelectric points (IEPs) of the membrane surfaces, where they carry no charge.

288 The IEP of TFC membrane occurs at pH 5, and the IEPs of the TFN membranes generally shift to

289 lower pH following the addition of GO into the PA layer because of the increasing quantity of

290 acidic groups from GO [20, 52]. The TFN0 membrane exhibits an increase in zeta potential

291 between pH 7 and 9 due to the presence of PMA in AQN. PMA increases the pH of the AQN

292 solution to 9 and alters the TFN0 membrane's zeta potential under high pH when it is incorporated

293 into the PA layer. Generally, the changes in membrane surface properties after addition of AQN

16

294 and GO flakes in the PA layer confirmed that the properties of the PA TFC membranes could be

295 regulated by altering the composition of the GO flakes and AQNs in the PA active layer.

296
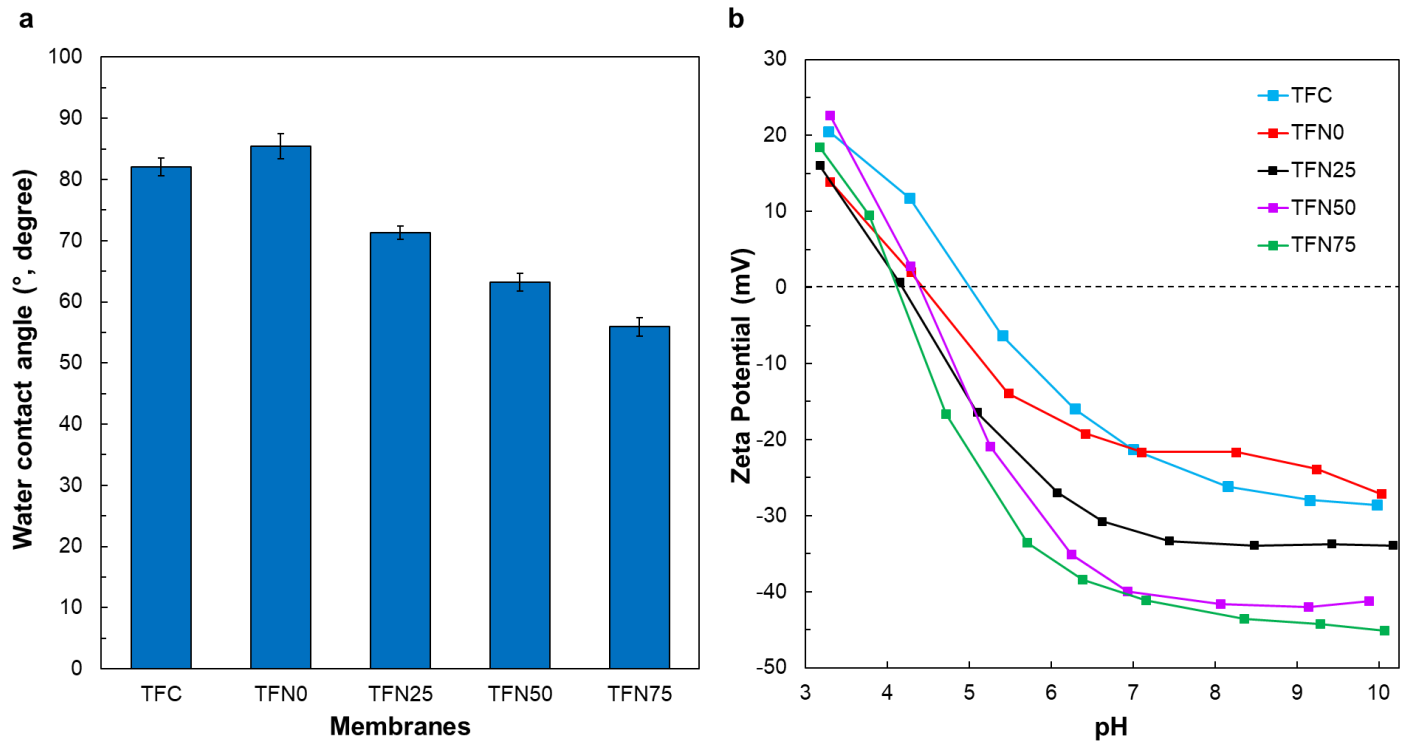
297

298 **Fig. 5**: (a) Water contact angle and (b) zeta potential measurements of the pristine TFC and
299 modified TFN membrane surfaces. Error bars for water contact angle measurements represent one
300 standard error obtained from at least seven measurements for each membrane sample.

301

302 **3.2   Membrane performance evaluation**

303   The FO performances of the membranes were evaluated from the water flux and *SRSF* values

304 obtained in AL-FS mode using 0.5 M NaCl as DS and DI water as FS (**Fig. 6**). The AQN-

305 embedded TFN membrane (TFN0) showed only a slight improvement in water flux (9.4 L.m^{-2}.h^{-}

306 ^{1}) compared to the pristine TFC membrane (8.2 L.m^{-2}.h^{-1}). However, TFN0 exhibited a 59%

17

307   reduction in *SRSF* (0.16 g.L^{-1}) than that of the TFC membrane (0.39 g.L^{-1}). This observation

308   confirms that AQN plays a role in improving the selectivity of the PA TFN membranes. We

309   speculate that AQN incorporation reduces the cross-linking density of the PA, as AQNs are

310   covalently bonded to the PA. Reduced cross-linking density is generally expected to reduce the

311   membrane selectivity; however, TFN0 membrane exhibited enhanced water permeability and

312   selectivity. Based on previous studies, incorporation of AqpZ or polymersomes/nanostructures is

313   known to improve membrane permeability [53-57]. The improved selectivity of the TFN0

314   membrane suggests that the addition of AQN retained the integrity of the PA layer and created

315   minimal or no PA defects. The slight improvement in the water flux of the TFN0 membrane can

316   be attributed to the AqpZ protein and the comparatively thinner PA layer (**Fig. 3**b and **Fig. 4**),

317   which facilitated faster water transport across the membrane.

318   On the other hand, both the water flux and *SRSF* across the AQN-incorporated TFN

319   membranes increased with increasing GO addition (TFN25, TFN50 and TFN75) compared to the

320   TFN0 membrane. The higher water flux of the AQN-GO incorporated TFN membranes could be

321   ascribed to their thinner and sparser PA layers (**Fig. 3**c-e and **Fig. 4**), which reduced the water

322   transport resistance across the membrane, and to their improved surface wettability (**Fig. 5**a). The

323   *SRSF* values of the AQN-GO incorporated TFN membranes increased at higher GO loadings due

324   to more defects formed in the PA layer, as discussed in our previous study [20]. The loose pore

325   structure of the PA layer at the highest GO loading of 75 mg.L^{-1} (TFN75) permitted relatively

326   more solute molecules to move from the DS to the FS. Nonetheless, it is interesting to note that

327   the selectivity of AQN-GO incorporated TFN membranes is much better than that of the GO-only

328   incorporated TFN membranes (TFNGO25, TFNGO50 and TFNGO75). Some of the non-selective

329   PA defects in GO TFN membranes, which formed due to GO restricting the IP reaction, could be

18

330   healed by reacting the exposed carboxyl groups with the amine groups of PMA chains in the AQNs.

331   In addition, the amphiphilic composition of the AQN may enhance the MPD diffusion during the

332   IP reaction, further improving selectivity and healing the defects induced by GO. The intrinsic

333   selectivity of the AQNs, coupled with the disappearance of some of the defects, is responsible for

334   the superior selectivity of the AQN-GO TFN membranes compared to the GO TFN membranes.

335   The performance results showed that AQNs could not completely eradicate PA defects formed by

336   GO. Nevertheless, overall results suggest that AQNs in PA help to partially heal the defects created

337   by GO in the PA layer. For instance, the TFN50 membrane (0.2 wt% AQN and 0.005 wt% GO)

338   exhibited a 27% lower *SRSF* than that of the TFNGO50 membrane (0.005 wt% GO) while

339   revealing similar water fluxes of ~23.5 $L.m^{-2}.h^{-1}$. The GO-incorporated TFN membranes

340   demonstrated nearly similar water flux as that of the AQN-GO incorporated TFN membranes at

341   the same GO loading, but those incorporated with AQN attained better selectivity to draw solutes.

342   The TFN50 membrane was selected as the optimum membrane for this study as it exhibited

343   substantial improvement in water flux with similar *SRSF* value as that of the pristine membrane.

344
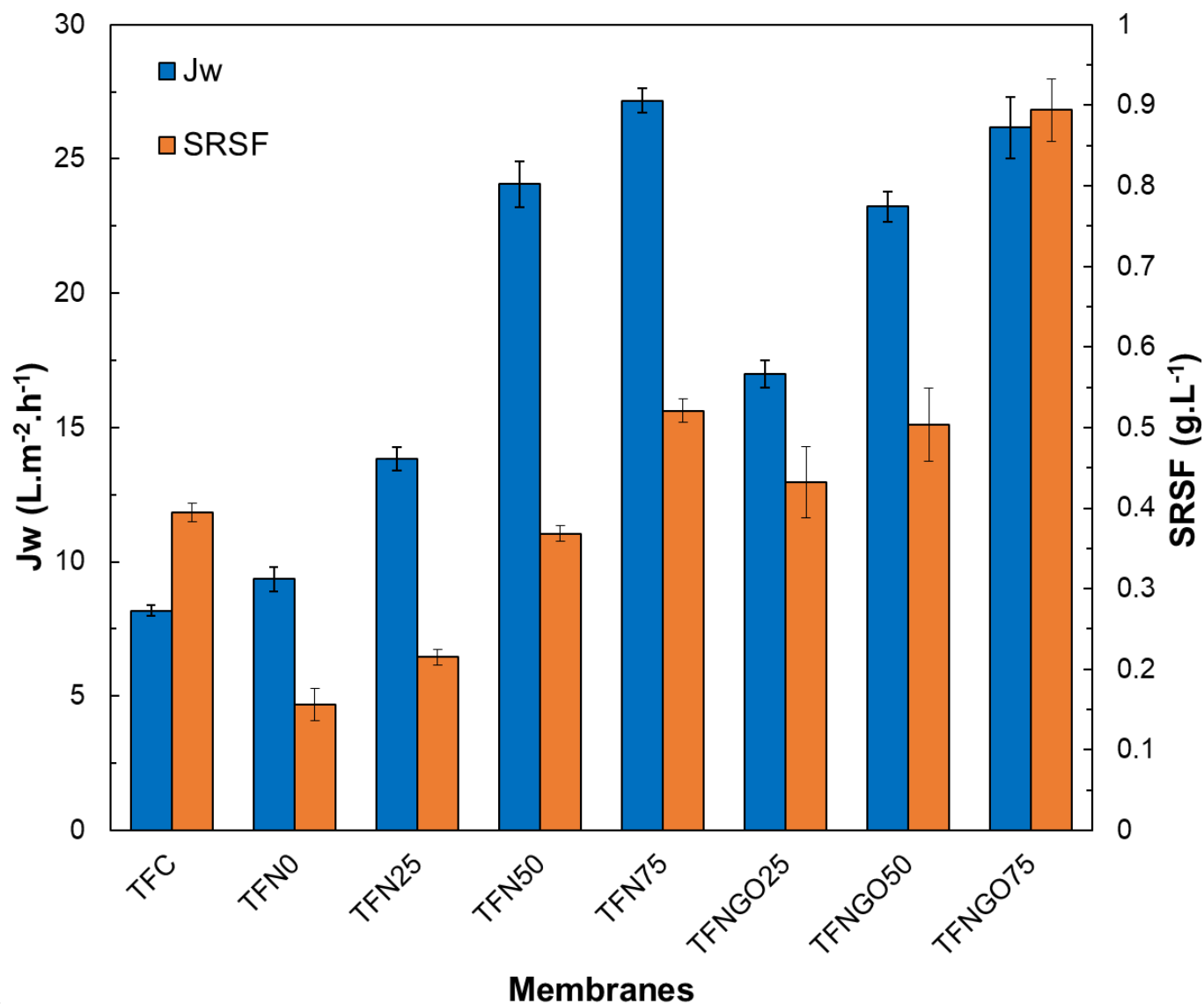
Fig. 6: FO performance of the pristine TFC and modified TFN membranes. Operating conditions: membrane orientation, AL-FS; DS, 0.5 M NaCl; FS, DI water; cross-flow velocity, 12.6 cm.s^{-1}. Error bars represent one standard error obtained from the performance test results of at least three membrane samples for each condition.

The intrinsic membrane transport properties were estimated from the *A* and *B* values as presented in **Table 2**. All the TFN membranes exhibited higher *A* values; whereas, TFN0 and TFN25 showed lower *B* values in comparison to the pristine membrane. The GO flakes improved

20

354 the membrane permeability by increasing membrane wettability, decreasing PA layer thickness

355 and creating defects in the PA layer; whereas, AQNs enhanced membrane selectivity by healing

356 PA defects. The *B/A* ratios of the prepared membranes are also shown in **Table 2**, where a smaller

357 *B/A* ratio represents a more selective membrane and vice versa. The TFN75 membrane showed the

358 highest *B/A* ratio of 0.63 bar; whereas, TFN0 was found to be the most selective by demonstrating

359 the smallest *B/A* value of 0.19 bar. The intrinsic transport parameters agree well with the FO

360 performance results displayed in **Fig. 6** and validated that the TFN membrane performance can be

361 adjusted by varying the AQN and GO concentrations in the PA layer. Additionally, the enhanced

362 selectivity of AQN-incorporated TFN membranes indicates that AQNs play an essential role in

363 repairing the PA defects.

364

365 **Table 2**: Intrinsic transport parameters of the membranes.

Membrane	A $(L.m^{-2}.h^{-1}.bar^{-1})$	B $(L.m^{-2}.h^{-1})$	*B/A* (bar)
TFC	1.02	0.47	0.46
TFN0	1.13	0.21	0.19
TFN25	1.59	0.41	0.26
TFN50	2.78	1.21	0.44
TFN75	3.06	1.93	0.63

366

367 **4   Conclusions**

368   In this study, TFN membranes were developed by incorporating both AQNs and GO flakes

369 in the PA layers to improve the separation performance of the TFN membranes. Addition of AQNs

21

370 in the TFN membranes improved the selectivity of the TFN membranes compared to the pristine

371 TFC membrane. While the addition of GO enhanced the membrane permeability and reduced the

372 membrane selectivity by creating non-selective defects in PA layer. However, addition of AQN

373 together with GO led to synergies with AQN healing the PA defects formed by GO; thus,

374 ultimately resulting in the development of promising PA TFN FO membranes with improved water

375 flux and low *SRSF*. The selective characteristic of AQNs led to enhanced membrane selectivity,

376 while GO improved the membrane surface wettability and water permeability. The TFN50

377 membrane with a GO and AQN loading of 0.005 wt% and 0.2 wt%, respectively, was found to be

378 the optimum membrane in this study as it demonstrated the highest water flux with a *SRSF* value

379 lower than that of the TFC membrane. The TFN50 membrane exhibited ~3 times higher water flux

380 $(24.1 \text{ L.m}^{-2}.\text{h}^{-1})$ than that of the pristine TFC membrane $(8.2 \text{ L.m}^{-2}.\text{h}^{-1})$ with similar *SRSF* values

381 using 0.5 M NaCl as DS and DI water as FS. Consequently, the synergy between AQN and GO

382 demonstrated in this study could be used to effectively heal the non-selective membrane defects

383 and improve the separation performance of the GO-incorporated PA TFN membranes for potential

384 application in desalination and wastewater reclamation. Moreover, this study provides a guideline

385 for future studies aiming to explore the synergistic use of different nanostructures/nanomaterials

386 for the preparation of novel membrane materials.

387

388

CRediT authorship contribution statement

Nawshad Akther: Conceptualization, Data curation, Formal analysis, Investigation, Methodology, Validation, Writing - original draft. **Victoria Sanahuja-Embuena:** Formal analysis, Validation, Writing - review & editing. **Radosław Górecki:** Consultation of the data in regards to AQN, Writing – review & editing. **Sherub Phuntsho:** Co-supervision, Writing - review & editing**. Claus Helix-Nielsen:** Writing - review & editing. **Hokyong Shon:** Supervision, Project administration, Resources, Funding acquisition, Validation, Writing - review & editing.

Declaration of competing interest

The authors declare that they have no known competing financial interests or personal relationships that could have appeared to influence the work reported in this paper.

404   **References**

405   [1] P. Marchetti, M.F. Jimenez Solomon, G. Szekely, A.G. Livingston, Molecular separation with
406   organic solvent nanofiltration: a critical review, Chem Rev, 114 (2014) 10735-10806.
407   [2] C. Klaysom, T.Y. Cath, T. Depuydt, I.F. Vankelecom, Forward and pressure retarded osmosis:
408   potential solutions for global challenges in energy and water supply, Chem Soc Rev, 42 (2013)
409   6959-6989.
410   [3] N. Akther, A. Sodiq, A. Giwa, S. Daer, H.A. Arafat, S.W. Hasan, Recent advancements in
411   forward osmosis desalination: A review, Chemical Engineering Journal, 281 (2015) 502-522.
412   [4] S. Daer, N. Akther, Q. Wei, H.K. Shon, S.W. Hasan, Influence of silica nanoparticles on the
413   desalination performance of forward osmosis polybenzimidazole membranes, Desalination, 491
414   (2020) 114441.
415   [5] V.H. Tran, S. Lim, D.S. Han, N. Pathak, N. Akther, S. Phuntsho, H. Park, H.K. Shon, Efficient
416   fouling control using outer-selective hollow fiber thin-film composite membranes for osmotic
417   membrane bioreactor applications, Bioresource Technology, 282 (2019) 9-17.
418   [6] N. Akther, S. Daer, S.W. Hasan, Effect of flow rate, draw solution concentration and
419   temperature on the performance of TFC FO membrane, and the potential use of RO reject brine as
420   a draw solution in FO–RO hybrid systems, Desalination and Water Treatment, 136 (2018) 65-71.
421   [7] V. Sant'Anna, L.D.F. Marczak, I.C. Tessaro, Membrane concentration of liquid foods by
422   forward osmosis: Process and quality view, Journal of Food Engineering, 111 (2012) 483-489.
423   [8] J. Zhang, Q. She, V.W.C. Chang, C.Y. Tang, R.D. Webster, Mining nutrients (N, K, P) from
424   urban source-separated urine by forward osmosis dewatering, Environmental Science &
425   Technology, 48 (2014) 3386-3394.
426   [9] N. Akther, S. Daer, Q. Wei, I. Janajreh, S.W. Hasan, Synthesis of polybenzimidazole (PBI)
427   forward osmosis (FO) membrane and computational fluid dynamics (CFD) modeling of
428   concentration gradient across membrane surface, Desalination, 452 (2019) 17-28.
429   [10] A. Tiraferri, C.D. Vecitis, M. Elimelech, Covalent binding of single-walled carbon nanotubes
430   to polyamide membranes for antimicrobial surface properties, ACS Applied Materials & Interfaces,
431   3 (2011) 2869-2877.
432   [11] A. Giwa, N. Akther, V. Dufour, S.W. Hasan, A critical review on recent polymeric and nano-
433   enhanced membranes for reverse osmosis, RSC Advances, 6 (2016) 8134-8163.
434   [12] N. Akther, S. Phuntsho, Y. Chen, N. Ghaffour, H.K. Shon, Recent advances in nanomaterial-
435   modified polyamide thin-film composite membranes for forward osmosis processes, Journal of
436   Membrane Science, 584 (2019) 20-45.
437   [13] X. Lu, L.H. Arias Chavez, S. Romero-Vargas Castrillón, J. Ma, M. Elimelech, Influence of
438   active layer and support layer surface structures on organic fouling propensity of thin-film
439   composite forward osmosis membranes, Environmental Science & Technology, 49 (2015) 1436-
440   1444.
441   [14] H. Maddah, A. Chogle, Biofouling in reverse osmosis: Phenomena, monitoring, controlling
442   and remediation, Applied Water Science, 7 (2017) 2637-2651.
443   [15] B.F. Jirjis, S. Luque, Chapter 9 - Practical aspects of membrane system design in food and
444   bioprocessing applications, in: Z.F. Cui, H.S. Muralidhara (Eds.) Membrane Technology,
445   Butterworth-Heinemann, Oxford, 2010, pp. 179-212.

446 [16] S. Lim, N. Akther, V.H. Tran, T.-H. Bae, S. Phuntsho, A. Merenda, L.F. Dumée, H.K. Shon,
447 Covalent organic framework incorporated outer-selective hollow fiber thin-film nanocomposite
448 membranes for osmotically driven desalination, Desalination, 485 (2020) 114461.
449 [17] B.H. Jeong, E.M.V. Hoek, Y. Yan, A. Subramani, X. Huang, G. Hurwitz, A.K. Ghosh, A.
450 Jawor, Interfacial polymerization of thin film nanocomposites: A new concept for reverse osmosis
451 membranes, Journal of Membrane Science, 294 (2007) 1-7.
452 [18] M.L. Lind, A.K. Ghosh, A. Jawor, X. Huang, W. Hou, Y. Yang, E.M.V. Hoek, Influence of
453 zeolite crystal size on zeolite-polyamide thin film nanocomposite membranes, Langmuir, 25 (2009)
454 10139-10145.
455 [19] X. Song, L. Wang, C.Y. Tang, Z. Wang, C. Gao, Fabrication of carbon nanotubes incorporated
456 double-skinned thin film nanocomposite membranes for enhanced separation performance and
457 antifouling capability in forward osmosis process, Desalination, 369 (2015) 1-9.
458 [20] N. Akther, Z. Yuan, Y. Chen, S. Lim, S. Phuntsho, N. Ghaffour, H. Matsuyama, H. Shon,
459 Influence of graphene oxide lateral size on the properties and performances of forward osmosis
460 membrane, Desalination, 484 (2020) 114421.
461 [21] S. Lim, K.H. Park, V.H. Tran, N. Akther, S. Phuntsho, J.Y. Choi, H.K. Shon, Size-controlled
462 graphene oxide for highly permeable and fouling-resistant outer-selective hollow fiber thin-film
463 composite membranes for forward osmosis, Journal of Membrane Science, (2020) 118171.
464 [22] S. Xu, F. Li, B. Su, M.Z. Hu, X. Gao, C. Gao, Novel graphene quantum dots (GQDs)-
465 incorporated thin film composite (TFC) membranes for forward osmosis (FO) desalination,
466 Desalination, 451 (2019) 219-230.
467 [23] Q. Shen, Y. Lin, Y. Kawabata, Y. Jia, P. Zhang, N. Akther, K. Guan, T. Yoshioka, H. Shon,
468 H. Matsuyama, Engineering heterostructured thin-film nanocomposite membrane with
469 functionalized graphene oxide quantum dots (GOQD) for highly-efficient reverse osmosis, ACS
470 Applied Materials & Interfaces, 12 (2020) 38662-38673.
471 [24] N. Niksefat, M. Jahanshahi, A. Rahimpour, The effect of SiO2 nanoparticles on morphology
472 and performance of thin film composite membranes for forward osmosis application, Desalination,
473 343 (2014) 140-146.
474 [25] N. Akther, S. Lim, V.H. Tran, S. Phuntsho, Y. Yang, T.-H. Bae, N. Ghaffour, H.K. Shon, The
475 effect of Schiff base network on the separation performance of thin film nanocomposite forward
476 osmosis membranes, Separation and Purification Technology, 217 (2019) 284-293.
477 [26] D. Ma, S.B. Peh, G. Han, S.B. Chen, Thin-film nanocomposite (TFN) membranes
478 incorporated with super-hydrophilic metal–organic framework (MOF) UiO-66: Toward
479 enhancement of water flux and salt rejection, ACS Applied Materials & Interfaces, 9 (2017) 7523-
480 7534.
481 [27] M. Amini, A. Rahimpour, M. Jahanshahi, Forward osmosis application of modified TiO2-
482 polyamide thin film nanocomposite membranes, Desalination and Water Treatment, 57 (2016)
483 14013-14023.
484 [28] E.E. McLeary, J.C. Jansen, F. Kapteijn, Zeolite based films, membranes and membrane
485 reactors: Progress and prospects, Microporous and Mesoporous Materials, 90 (2006) 198-220.
486 [29] K.A. Mahmoud, B. Mansoor, A. Mansour, M. Khraisheh, Functional graphene nanosheets:
487 The next generation membranes for water desalination, Desalination, 356 (2015) 208-225.
488 [30] S. Lim, K.H. Park, V.H. Tran, N. Akther, S. Phuntsho, J.Y. Choi, H.K. Shon, Size-controlled
489 graphene oxide for highly permeable and fouling-resistant outer-selective hollow fiber thin-film
490 composite membranes for forward osmosis, Journal of Membrane Science, 609 (2020) 118171.

491   [31] N. Akther, S.M. Ali, S. Phuntsho, H. Shon, Surface modification of thin-film composite
492   forward osmosis membranes with polyvinyl alcohol–graphene oxide composite hydrogels for
493   antifouling properties, Desalination, 491 (2020) 114591.
494   [32] A.S. Verkman, Aquaporins, Current Biology, 23 (2013) R52-R55.
495   [33] M.J. Borgnia, D. Kozono, G. Calamita, P.C. Maloney, P. Agre, Functional reconstitution and
496   characterization of AqpZ, the E. coli water channel protein11Edited by W. Baumeister, J. Mol.
497   Biol., 291 (1999) 1169-1179.
498   [34] A.S. Verkman, A.K. Mitra, Structure and function of aquaporin water channels, American
499   Journal of Physiology-Renal Physiology, 278 (2000) F13-F28.
500   [35] R. Górecki, D.M. Reurink, M.M. Khan, V. Sanahuja-Embuena, K. Trzaskuś, C. Hélix-Nielsen,
501   Improved reverse osmosis thin film composite biomimetic membranes by incorporation of
502   polymersomes, Journal of Membrane Science, 593 (2020) 117392.
503   [36] R. Sengur-Tasdemir, S. Aydin, T. Turken, E.A. Genceli, I. Koyuncu, Biomimetic approaches
504   for membrane technologies, Separation & Purification Reviews, 45 (2016) 122-140.
505   [37] L. Xia, M.F. Andersen, C. Hélix-Nielsen, J.R. McCutcheon, Novel commercial aquaporin
506   flat-sheet membrane for forward osmosis, Industrial & Engineering Chemistry Research, 56 (2017)
507   11919-11925.
508   [38] Y. Zhao, A. Vararattanavech, X. Li, C. HélixNielsen, T. Vissing, J. Torres, R. Wang, A.G.
509   Fane, C.Y. Tang, Effects of proteoliposome composition and draw solution types on separation
510   performance of aquaporin-based proteoliposomes: Implications for seawater desalination using
511   aquaporin-based biomimetic membranes, Environmental Science & Technology, 47 (2013) 1496-
512   1503.
513   [39] F. Itel, A. Najer, C.G. Palivan, W. Meier, Dynamics of membrane proteins within synthetic
514   polymer membranes with large hydrophobic mismatch, Nano Letters, 15 (2015) 3871-3878.
515   [40] M. Garni, S. Thamboo, C.-A. Schoenenberger, C.G. Palivan, Biopores/membrane proteins in
516   synthetic polymer membranes, Biochimica et Biophysica Acta (BBA) - Biomembranes, 1859
517   (2017) 619-638.
518   [41] D.E. Discher, A. Eisenberg, Polymer vesicles, Science, 297 (2002) 967.
519   [42] D.E. Discher, F. Ahmed, Polymersomes, Annual Review of Biomedical Engineering, 8 (2006)
520   323-341.
521   [43] W. Xie, F. He, B. Wang, T.-S. Chung, K. Jeyaseelan, A. Armugam, Y.W. Tong, An
522   aquaporin-based vesicle-embedded polymeric membrane for low energy water filtration, Journal
523   of Materials Chemistry A, 1 (2013) 7592-7600.
524   [44] M. Grzelakowski, K. Kita-Tokarczyk, Terminal groups control self-assembly of amphiphilic
525   block copolymers in solution, Nanoscale, 8 (2016) 6674-6683.
526   [45] M. Spulber, D.C. Tvermoes, R. Gorecki, F. Haugsted, Vesicle incorporating transmembrane
527   protein, in: W.I.P. Organization (Ed.), 2019.
528   [46] C.Y. Tang, Y.-N. Kwon, J.O. Leckie, Effect of membrane chemistry and coating layer on
529   physiochemical properties of thin film composite polyamide RO and NF membranes: I. FTIR and
530   XPS characterization of polyamide and coating layer chemistry, Desalination, 242 (2009) 149-167.
531   [47] Y. Hu, K. Lu, F. Yan, Y. Shi, P. Yu, S. Yu, S. Li, C. Gao, Enhancing the performance of
532   aromatic polyamide reverse osmosis membrane by surface modification via covalent attachment
533   of polyvinyl alcohol (PVA), Journal of Membrane Science, 501 (2016) 209-219.

534 [48] Y. Kang, M. Obaid, J. Jang, I.S. Kim, Sulfonated graphene oxide incorporated thin film
535 nanocomposite nanofiltration membrane to enhance permeation and antifouling properties,
536 Desalination, 470 (2019) 114125.
537 [49] J. Yin, G. Zhu, B. Deng, Graphene oxide (GO) enhanced polyamide (PA) thin-film
538 nanocomposite (TFN) membrane for water purification, Desalination, 379 (2016) 93-101.
539 [50] M. Rastgar, A. Shakeri, A. Bozorg, H. Salehi, V. Saadattalab, Highly-efficient forward
540 osmosis membrane tailored by magnetically responsive graphene oxide/Fe3O4 nanohybrid,
541 Applied Surface Science, 441 (2018) 923-935.
542 [51] W.J. Lau, A.F. Ismail, P.S. Goh, N. Hilal, B.S. Ooi, Characterization methods of thin film
543 composite nanofiltration membranes, Separation & Purification Reviews, 44 (2015) 135-156.
544 [52] A.M. Dimiev, L.B. Alemany, J.M. Tour, Graphene Oxide. Origin of Acidity, Its Instability in
545 Water, and a New Dynamic Structural Model, ACS Nano, 7 (2013) 576-588.
546 [53] S. Qi, W. Fang, W. Siti, W. Widjajanti, X. Hu, R. Wang, Polymersomes-based high-
547 performance reverse osmosis membrane for desalination, Journal of Membrane Science, 555 (2018)
548 177-184.
549 [54] Y. Li, S. Qi, M. Tian, W. Widjajanti, R. Wang, Fabrication of aquaporin-based biomimetic
550 membrane for seawater desalination, Desalination, 467 (2019) 103-112.
551 [55] C. Tang, Z. Wang, I. Petrinić, A.G. Fane, C. Hélix-Nielsen, Biomimetic aquaporin
552 membranes coming of age, Desalination, 368 (2015) 89-105.
553 [56] M. Kumar, M. Grzelakowski, J. Zilles, M. Clark, W. Meier, Highly permeable polymeric
554 membranes based on the incorporation of the functional water channel protein Aquaporin Z,
555 Proceedings of the National Academy of Sciences, 104 (2007) 20719-20724.
556 [57] H.X. Gan, H. Zhou, H.J. Lee, Q. Lin, Y.W. Tong, Toward a better understanding of the nature-
557 inspired aquaporin biomimetic membrane, Langmuir, 35 (2019) 7285-7293.

558